Microwaves used for the first time in the position control of a fusion machine

Jorge Santos
(Project Principal Investigator)
Associação EURATOM/IST
Instituto de Plasmas e Fusão Nuclear
Instituto Superior Técnico
Universidade Técnica de Lisboa
1049-001 Lisboa, Portugal
Email: jsantos@ipfn.ist.utl.pt

L. Guimarãis, M. Manso, and the
IPFN Microwave Diagnostics Group
Associação EURATOM/IST
Instituto de Plasmas e Fusão Nuclear
Instituto Superior Técnico
Universidade Técnica de Lisboa
1049-001 Lisboa, Portugal

M. Zilker, W. Treutterer,
and the ASDEX Upgrade Team
Max-Planck Institut für Plasmaphysik
EURATOM Association
D-85748 Garching, Germany

***Abstract*—With the present construction, in France, of the International Thermonuclear Experimental Reactor (ITER), nuclear fusion, one of the more promising solutions for the sustainable large scale production of energy, is one step closer of becoming a player in the future energy mix. In ITER and in future commercial fusion reactors, highly energetic nuclear fusion reactions will be produced when a deuterium and tritium (D-T) plasma is heated up to temperatures ten times higher than the Sun's core temperature. The position control of this extremely hot column of plasma, inside the reactor's fusion chamber, is one of the most critic issues in the operation of these power generating devices. So far, real-time feedback systems used magnetic measurements to determine and control the plasma position. However, during the reactor's long pulse operation, the fast neutrons and radiation emitted by D-T plasmas may affect the magnetic sensors, likely leading to the accumulation of errors in the feedbacked measurements.**

Microwave reflectometry, a radar technique for determining the radial distribution of the plasma density, was proposed to provide an alternative to the magnetic measurements used for position control. However, producing reliable measurements from waves propagating in a turbulent fusion plasma has proved to be a difficult and complex task that needed to be successfully tamed before being validated as an alternative for measuring the plasma position. Herein are described the developments required to integrate this radar-like technique in the control systems of a fusion machine. These developments led to the first demonstration of plasma position control made in a fusion device using an alternative to the usual feedback of magnetic measurements. This ITER relevant demonstration was performed in the second largest European machine, the ASDEX Upgrade tokamak, located in Garching, Germany.

I. Introduction

In the plasma fusion community microwave reflectometry is a well proven radar like technique used for producing different types of physics measurements. The turbulence characteristics of fixed electron density layers can be studied by continuously probing the plasma with waves of fixed frequency. By carefully selecting the incidence/reflection angles of such waves, and using the Doppler effect, the measurements of the poloidal velocity of the probed corrugated plasma surfaces can be used to calculate the plasma radial electric field. If the frequency of the incident probing waves is swept, the position of the density layers, at which the corresponding reflections occur, can be obtained from the measured waves' group delay. This information can then be used to calculate a density profile along the reflectometer's line of sight.

Of the mentioned techniques we will only address the latter and the developments required to turn the existing ASDEX Upgrade[1] (AUG) FMCW reflectometry system [1] into a real-time diagnostic used for plasma position feedback control [2]. The demonstration of this novel control technique was considered most relevant for the ITER[2] project, as the plasma position controllers are the systems that guarantee that the very hot fusion plasma does not touch and destroy the inner tokamak plasma facing components. For this reason, the European Fusion Development Agreement (EFDA) awarded priority support financing to the developments and the demonstration experiments herein described.

Today, the tokamak's real-time (RT) feedback systems use magnetic measurements of the plasma boundary location to perform plasma position control. During the long pulse operation of future fusion devices, however, these measurements may be affected by drifting integrators or radiation induced voltages in the magnetic pickup coils. Therefore, to complement the magnetic data, a set of frequency modulated continuous wave (FMCW) plasma position reflectometers (PPR) is being designed for ITER. Operating in O-mode, these reflectometers will provide, at four defined locations (known as Gaps 3, 4, 5 and 6 - see Fig. 1), measurements of the edge density profile as well as the distance between the first wall and the separatrix[3]. The latter can be used to correct drifts in the magnetic measurements during ITER long pulses or to directly control the plasma, independently of the magnetics. The implementation of this new concept for control required

[1]The ASDEX Upgrade tokamak, located in Garching, is Germany's largest fusion device. See: www.ipp.mpg.de.

[2]The International Tokamak Experimental Reactor (ITER) is the world's largest Tokamak under construction in Cadarache France. In this future tokamak will be produced for the first time sustained reactor grade fusion plasmas. See http://www.iter.org

[3]The separatrix is the last-closed magnetic flux surface (magenta line in the tokamak cut views of Fig. 1).

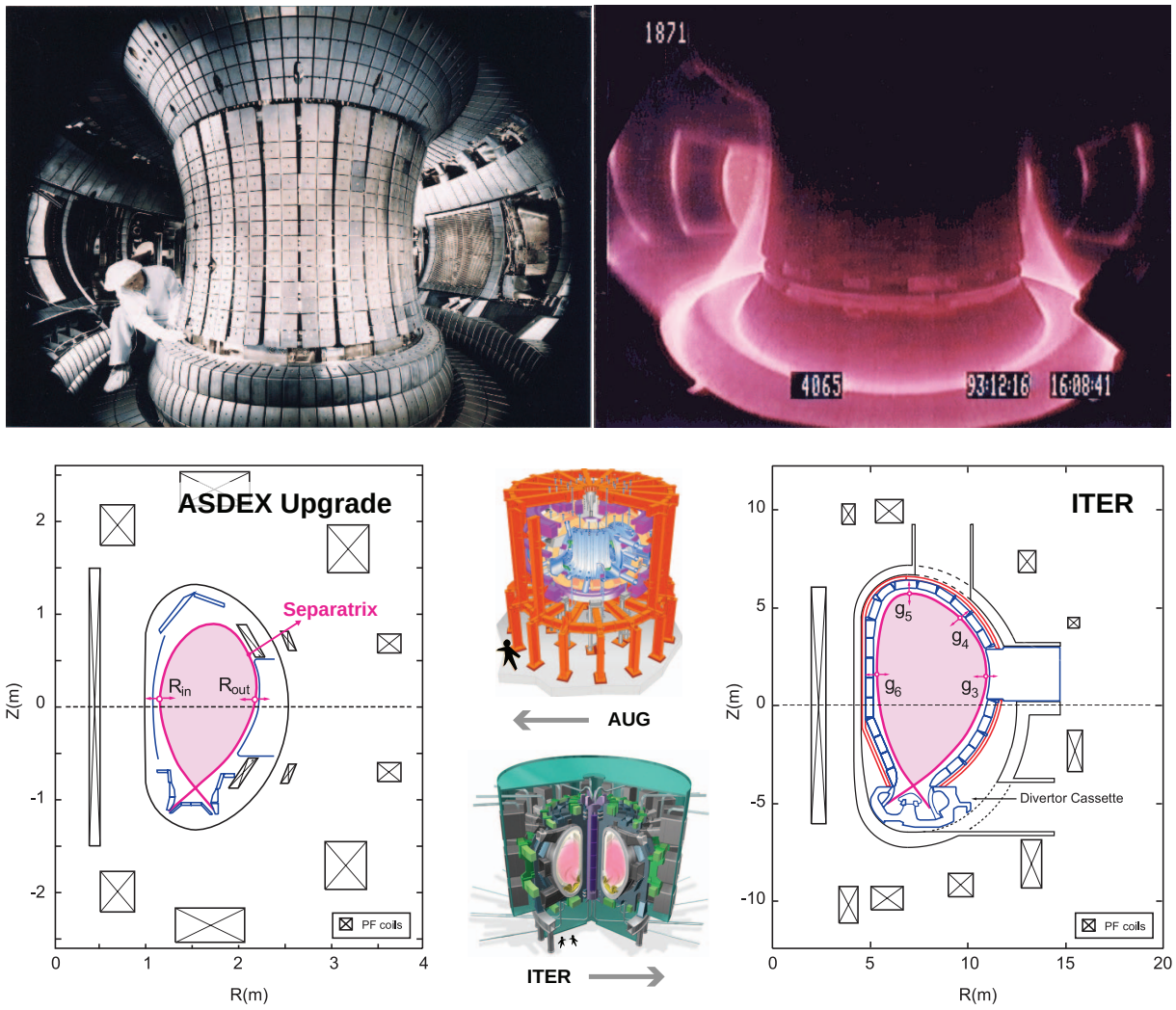

Fig. 1. Inner view of the toroidal plasma chamber of the ASDEX Upgrade (AUG) tokamak (top left) and of the plasma typical pink glow during a discharge (top right). Schematic views of both AUG and ITER, showing the structure supporting the plasma vessel, access ports and poloidal field (PF) coils (central column). Poloidal cut views of the AUG and ITER tokamaks and the magnetic separatrix gaps monitored by the respective plasma position reflectometers: R_{in} and R_{out} on AUG, and $g_{3,4,5,6}$ on ITER (side plots).

a practical validation on an ITER relevant fusion device. For this purpose, a full feedback control demonstration has been conducted for the first time at the AUG tokamak, using its O-mode reflectometers in a setup similar to ITER's[4]. The reflectometry's complex microwave signal analysis, used for many years to measure the density profile, was not sufficiently robust to produce automated measurements for control purposes. The recent upgrades introduced on the AUG reflectometry system together with a matured innovative data processing technique allowed for a successful position control demonstration, in ITER relevant plasma regimes. Brief overviews of the reflectometry measurement principle, developed real-time algorithms, experimental setup and finally of the resulting control performance will be presented in the following sections.

[4]The AUG O-mode reflectometers are able to monitor the separatrix to wall gaps at two positions, i.e. R_{in} and R_{out}, that are very similar to the gaps g_3 and g_6 to be monitored on ITER (see Fig. 1).

II. Probing Plasmas with Microwave Reflectometry

Radio frequency (RF) techniques used to actively probe the plasma are at the basis of an important group of modern measurement diagnostics. Due to the low amplitudes of the used probing waves the perturbations introduced in the plasma are negligible. However, from the interaction between the propagating wave's electromagnetic field and the magnetized plasma result changes in its amplitude, phase, polarization state and spectrum. All these measurable effects can be used for diagnostic purposes. In particular, the fact that the probing waves are reflected at specific cut-off density layers, allows the calculation of their location from the measurable wave round trip delay. This is the principle used to reconstruct the electron density profiles from which the location of the separatrix is to be estimated in real-time.

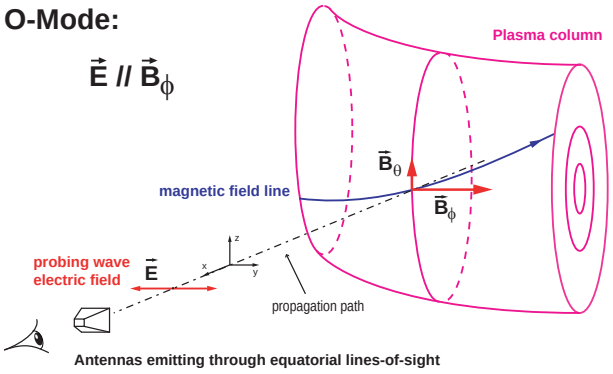

Fig. 2. O-mode propagation in a plasma.

A. Measurement principle

The propagation of electromagnetic waves in an inhomogeneous medium, like a fusion plasma, can be described using both the Maxwell equations and the motion equations of its particles. This description is possible if we assume [3] that: in the absence of electromagnetic perturbations the plasma particles stay in their equilibrium positions (cold plasma approximation); the plasma can be considered as a fluid of ions and electrons coupled through the wave electromagnetic field (fluid approximation); only the electrons are considered to contribute to the media polarization since the frequency of the electromagnetic wave is much higher than the plasma ion cyclotron and ion plasma frequencies (high frequency approximation); the plasma is homogeneous in all the directions except the wave propagation one (stratified media approximation). Assuming the former approximations and considering a wave propagation direction perpendicular to the plasma magnetic field ($\mathbf{k} \perp \mathbf{B}$, where $\mathbf{k}$ is the propagation direction and $\mathbf{B}$ the plasma magnetic field), two propagation modes can be defined [4]: the *ordinary mode* (**O-mode**), Fig. 2, where the wave's electric field is parallel to the plasma magnetic field ($\mathbf{E} \parallel \mathbf{B}$) and the extraordinary mode (X-mode), where the electric field of the wave is perpendicular to the magnetic field of the plasma ($\mathbf{E} \perp \mathbf{B}$). In a tokamak plasma, we just consider the toroidal component of the magnetic field, i.e. $\mathbf{B} \simeq \mathbf{B}_\phi$, the poloidal component is comparably negligible ($\mathbf{B}_\phi \gg \mathbf{B}_\theta$).

The refractive index for an O-mode wave with frequency f, N_O, is given by[5] [5]:

$$N_O = \left[1 - (f_{pe}/f)^2\right]^{1/2} = \left[1 - n_e/n_{co}\right]^{1/2} \quad (1)$$

where n_e is the electron density, and $f_{pe} = (n_e\, e^2/\varepsilon_0 m_e)^{1/2}/2\pi$ the electron plasma frequency. Wave propagation is possible for $f > f_{pe}$ or for $n_e < n_{co}$, where the cut-off density is given by:

$$n_{co} = (2\pi f/e)^2 \varepsilon_0 m_e \quad (2)$$

[5]Where e is the electron charge, m_e is the electron mass and ε_0 is the permittivity of free space.

In X-mode, the wave is elliptically polarized in the plasma and has an electric field component in the propagation direction as well as one in a direction normal to it. In this case, with the plasma electron cyclotron frequency given by $f_{ce} = eB/(2\pi m_e)$, the refractive index becomes:

$$N_X = \left[1 - \left(\frac{f_{pe}}{f}\right)^2 \frac{f^2 - f_{pe}^2}{f^2 - (f_{pe}^2 - f_{ce}^2)}\right]^{1/2} \quad (3)$$

As can be seen, only O-mode measurements are unaffected by the magnetic field being therefore independent from information originating in the magnetic diagnostics. This is the main reason for which stand-alone O-mode reflectometers were chosen to build a redundant plasma position controller capable of complementing or replacing the standard magnetic based controller.

In practice, a microwave reflectometer works like a radar: a wave with frequency f is launched to the plasma, propagating through it as long as its density is smaller than the cut-off density $n_{co}(f)$. When reaching the cut-off layer, the refraction index becomes zero and the wave is reflected. The wave suffers a total phase shift on the round-trip which is equivalent to the time delay of a returning radar echo. The temporal variation of its phase, ϕ, can result either from the variation of the probing frequency or of the optical path length $\int_0^{x_{co}} N_O(f,x)dx$, between the antenna position, at $x = 0$, and the reflecting layer, at $x = x_{co}$, where $N_O(f,x)$ is the refraction index along the line of sight. Temporal changes of the phase are given by[6]:

$$\begin{aligned}\frac{\partial \phi}{\partial t} &= \frac{4\pi}{c}\left(\frac{\partial f}{\partial t}\right)\int_{x=0}^{x_{co}} N_O(f,x)dx + \\ &+ \frac{4\pi}{c} f \frac{\partial}{\partial t}\left(\int_{x=0}^{x_{co}} N_O(f,x)dx\right)\end{aligned} \quad (4)$$

The position of the reflecting layer can be determined using the first term of the sum by simply sweeping the probing frequency and measuring $\partial\phi/\partial f$ or, equivalently, the corresponding probing waves group delay:

$$\tau_g = (2\pi)^{-1}(\partial\phi/\partial f) \quad (5)$$

The second term in equation (4) describes phase changes introduced by variations of the optical path length that arise from temporal and spatial fluctuations of the plasma electron density.

Considering only the first term of (4), the position $x_{co}(f_{co})$ of the reflecting layer with cut-off frequency f_{co} can be recovered analytically performing an Abel inversion [6]:

$$x_{co}(f_{co}) = \frac{c}{\pi}\int_0^{f_{co}} \frac{\tau_g(f)}{\sqrt{f_{co}^2 - f^2}} df \quad (6)$$

[6]The application of the Maxwell equations to the propagation of electromagnetic waves in inhomogeneous mediums does not lead to an exact solution. The **WKB** (Wentzel, Kramers and Brillouin) approximation [4] is used instead, being valid if the (vacuum) probing wavelength, λ_0, is smaller than the density gradient characteristic length, L, where $L = [1/n(dn/dr)]^{-1}$ [6].

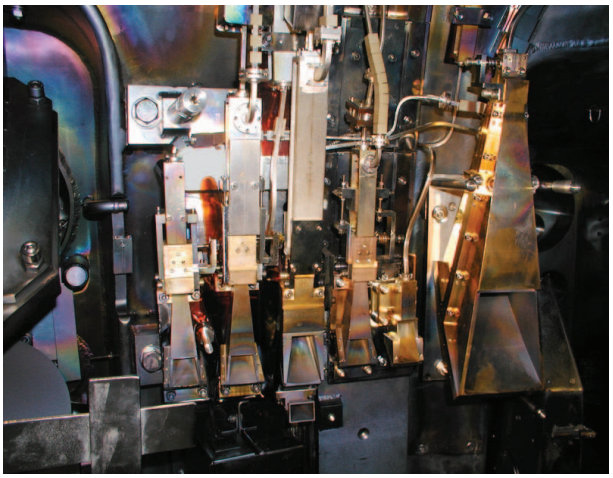

Fig. 3. LFS antenna array with the frontal protecting shielding plate removed.

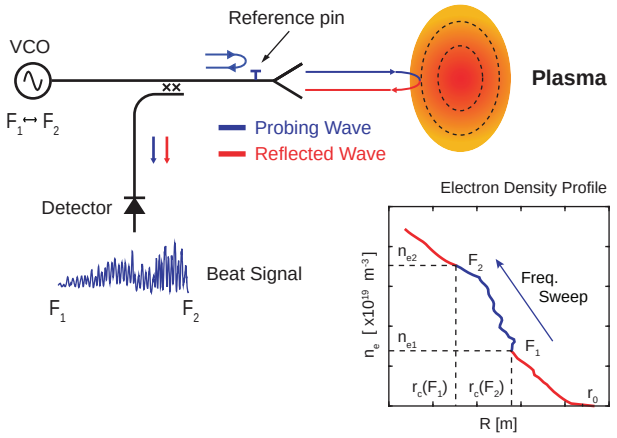

Fig. 4. Simplified working schematic of the ASDEX Upgrade reflectometry density profile measurement diagnostic.

provided $\tau_g(f)$ is known with sufficient accuracy to perform the integration.

B. FMCW density profile measurements on ASDEX Upgrade

The AUG broadband reflectometry diagnostic entered operation in the early 1990's. The system was designed by the IPFN/IST Microwave Diagnostics Group (MDG) and is operated by the group in close collaboration with the hosting ASDEX Upgrade Team, of the Max-Planck Institut fuer Plasmaphysik (IPP). In this experiment, two FMCW O-mode reflectometry systems [1] probe the plasma at the tokamak equatorial plane, from the high and low magnetic field sides[7] (HFS and LFS, respectively) of the machine. The HFS reflectometers operate in the $\approx 17-70$ GHz frequency ranges (bands K, Ka, Q and V). In the LFS, this range is extended, up to ≈ 100 GHz, with an additional reflectometer operating in the W band. In the LFS two additional channels operating in X-mode cover the $\approx 35-70$ GHz range (bands Q and V).

On its conception, the system was highly conditioned by the reduced space available inside the tokamak to route wave guides and place antennas behind the vessel heat shield[8].

These constraints and the previous experience gained with the reflectometers built for the old ASDEX tokamak led to an optimized design using focused hog-horn antennas (see Fig. 3) in a mono-static arrangement (a single antenna is used to emit and receive). Such arrangement allows for a more compact solution, specially on the HFS[9] were the space is even more restricted. As depicted in Fig. 4, a fraction of the emitted signal is reflected at a metallic pin, generating a reference that will be mixed with the plasma reflected signal at a waveguide mounted Shotky-diode detector. A directional coupler is used to separate the emitted and received signals. The higher bands, V and W, that probe plasma layers more distant from the antennas, were later upgraded to increase the system's SNR. This upgrade involved the use of an heterodyne detection scheme with a phase-locked-loop (PLL) and a second oscillator to drive an harmonic mixer to down-convert the reflected signals to an intermediate frequency (IF). In these channels the IF signal is still detected with a Shotky-diode detector (at about 1 GHz).

[7]These coincide with the inner and outer sides of the tokamak vessel where the plasma is produced.

[8]The heat shield is made of heat resistant tiles that protect the inner vessel walls and all the plasma facing components (See top left photo of Fig. 1).

[9]Due to its design, the AUG reflectometry system is the only diagnostic in the world capable of directly probing the plasma from the machine HFS.

Probing the plasma

To measure a density profile, a density range $[n_{e1}, n_{e2}]$ is scanned by continuously modulating the frequency of a microwave source (VCO of Fig. 4) in a corresponding range $[F_1, F_2]$. The relation between the generated chirp instantaneous frequency and the density being probed is given by (2). The probing signal, $s_p(t)$, emitted to the plasma can be written as:

$$s_p(t) = a_p(t)\cos[\theta(t)] \tag{7}$$

It's phase, $\theta(t)$, is given by

$$\theta(t) = 2\pi\left[F_1 t + k_v \int_0^t m(\lambda)d\lambda\right] \tag{8}$$

where F_1 is the initial frequency, k_v (Hz/V) is the VCO frequency sensitivity and $m(t)$ is the VCO input signal.

The VCO instantaneous frequency is then

$$f_p(t) = \frac{1}{2\pi}\frac{d\theta}{dt} = F_1 + k_v m(t) \tag{9}$$

Assuming that $m(t)$ is a ramp, i.e., $m(t) = \mu t$, $t \geq 0$, the frequency will be swept linearly in time

$$f_p(t) = F_1 + k_{sw} t = F_1 + \frac{(F_2 - F_1)}{T_{sw}} t \tag{10}$$

where the frequency sweep rate is $k_{sw} = k_v \mu$, T_{sw} is the full sweep duration or period, F_2 is the final frequency. In this case, $\theta(t)$ becomes

$$\theta(t) = 2\pi F_1 t + \pi k_{sw} t^2 \tag{11}$$

The signal $s_p(t)$ is partially reflected at the antenna pin to provide a reference signal that will add to the signal reflected in the plasma, $s_r(t)$

$$s_r(t) = a_r(t)\cos[\theta(t - \tau_g(t))] \tag{12}$$

where $\tau_g(t)$ is the delay of $s_r(t)$ regarding $s_p(t)$.

As mentioned before, the AUG reflectometer use a square-law mixer [7] as a signal detector. This type of mixer is implemented using a *Silicon Low Barrier Schottky Diode* [8], operating in the square-law region of its transfer function.

The baseband component resulting from low-pass filtering the mixed signal is:

$$s_b(t) = s_{LF}(t) + A(t)\cos[\phi(t)] \tag{13}$$

where $s_{LF}(t) = (a_p(t)^2 + a_r(t)^2)/2$ (a DC/low frequency term) and $A(t) = a_p(t)a_r(t)$, both dependent on the amplitude envelopes of the probing and reflected waves. Even if the $s_{LF}(t)$ term is properly eliminated, $\phi(t)$ and $A(t)$ are still combined in the resulting beat signal. Therefore, the extraction of $\phi(t)$ from $s_b(t)$ requires more sophisticated processing algorithms to compensate the simplicity of the hardware implementation.

The group delay, $\tau_g(t)$, required to perform the density profile inversion (eq. (6)), is calculated using the estimated beat frequency, $f_b(t)$, of the detected signal:

$$\begin{aligned} f_b(t) &= \frac{1}{2\pi}\frac{\partial\phi}{\partial t} \\ &= F_1\frac{\partial\tau_g}{\partial t} + k_{sw}\left(t\frac{\partial\tau_g}{\partial t} + \tau_g(t)\right) - k_{sw}\tau_g(t)\frac{\partial\tau_g}{\partial t} \\ &= f_p(t)\frac{\partial\tau_g}{\partial t} + k_{sw}\tau_g(t)\left(1 - \frac{\partial\tau_g}{\partial t}\right) \end{aligned} \tag{14}$$

which, for typical values of $f_p(t)$ and $\partial\tau_g/\partial t$, is reasonable to simplify to (in agreement with [9]) :

$$f_b(t) \approx k_{sw}\tau_g(t) = \frac{df_p}{dt}\tau_g(t) \tag{15}$$

where df_p/dt is the sweeping rate of the probing waves. Because the VCO is not swept linearly in frequency, a post linearization [10] procedure is required so that the resulting signal is equivalent to the one that would be obtained by sweeping linearly the same ΔF_p probing range in a ΔT sweeping period. The sweeping rate becomes a constant, $\partial f/\partial t = \Delta F_p/\Delta T$, hence:

$$f(t) = \frac{\Delta F_p}{\Delta T}t + F_1 \tag{16}$$

being $\Delta F_p = F_2 - F_1$ and F_1 and F_2 the two extreme probing frequencies of the swept range. Eq. (15) can then be re-written as:

$$\tau_g(t) = f_b(t)\left(\frac{\Delta F_p}{\Delta T}\right)^{-1} \tag{17}$$

and directly used in eq. (6) to calculate the density profile.

The correct estimation of the evolution of the beat frequency is one of the most critical points in the reconstruction of the reflectometry density profile. This is particularly true because plasma fluctuations affect the wave's propagation (second term of eq. (4)), causing phase and amplitude modulations of the beat signal. To avoid these effects, the frequency sweep is performed on a time scale expected to be shorter than the time scale of the most significant motions of the cut-off layers. The spurious phase shifts induced by the plasma turbulence are then significantly reduced because the phase measurements are made on a quasistatic plasma.

Beat frequency analysis

The beat frequency, $f_b(t)$, is by definition the instantaneous frequency of the interference signal (eq. 14). Therefore, the task of evaluating $\tau_g(f)$ using eq. 17 becomes a classical frequency estimation problem applied to a non-stationary (reflectometry) signal [11].

Historically, the first approach to estimate the beat frequency of the interference signal was to perform manual fringe counting [6] in rudimentarily acquired swept signals. Electronic fringe counters were the natural successors [12] but with the availability of fast data acquisition systems these where replaced by similar software based techniques like *zero-crossing* counting or *minima/maxima* detection [13]. To overcome the weaknesses of such methods, these evolved into more sophisticated time-based techniques like the *frequency discriminator* [14] and the *complex demodulation* [15], [16]. However, the rich spectral content of the reflectometry signals, specially during more turbulent plasma regimes, motivated the use of time-frequency data analysis. These techniques resolve the spectral evolution in a time-frequency plane providing the needed insight to understand the signals that otherwise would be more or less "blindingly" processed using heavy filtering dependent time-based methods. Some of the tested techniques were the *spectrogram* [17], [18], the *maximum entropy method* [17], [19] and *wavelet* [20] and *Wigner-Ville* [21], [22] family of transforms.

After experimenting with most of the above mentioned methods, a spectrogram based technique was selected to obtain the beat frequency. This simple yet powerful time-frequency distribution (TFD), lends itself to very optimized and performant implementations, a major advantage for a RT control application. The spectrogram, $SPEC_h(t, f)$, is no more than the squared magnitude of the Short-time Fourier Transform ($STFT_h(t, f)$):

$$\begin{aligned} \mathbf{SPEC_h(t, f)} &= |STFT_h(t, f)|^2 \\ &= \left|\int_{-\infty}^{+\infty} s(\tau)h^*(\tau - t)\, e^{-j2\pi ft}\, d\tau\right|^2 \end{aligned} \tag{18}$$

In the discrete time domain, eq. (18) is calculated using the Fast Fourier Transform (FFT), an highly optimized algorithm to solve the discrete FT.

Before extracting the beat frequency from the spectrograms, the time-frequency data coming from the various microwave bands needs to be aggregated in a single multi-band TFD. As all of the bands are swept simultaneously, in the same amount of time, the corresponding frequency sweep rates, $\Delta F_p/\Delta T$, will be different. Furthermore, the physical characteristics of each individual reflectometer, such as the length of the internal microwave paths in vacuum from the pins up to the antennas mouths and the relative antenna positions in respect to the plasma, will also influence the actual beat frequency range produced by each reflectometer. For these reasons, the multi-band beat frequency information can only be aggregated in a common 2D representation in the group delay vs. probing frequency space, after all the relevant transformations and corrections have been factored in using:

$$\tau_g(t) = f_b(t)\left(\frac{\Delta F_p}{\Delta T}\right)^{-1} - \tau_{corr} \tag{19}$$

where τ_{corr} are the referred propagation in vacuum corrections. Fig. 5 graphically depicts the steps involved in building the final multi-band spectrogram. The axis of the spectrograms in Fig 5.b, obtained from the interference signals of the various bands, in Fig. 5.a, are transformed using eq. (19) to obtain the equivalent TFDs in the τ_g space of Fig. 5.c. These, in turn, are cropped to a common τ_g range and combined in the single resampled TFD of Fig. 5.d.

Extracting the beat frequency from the spectrogram

For low levels of plasma fluctuation the interference signal is essentially a mono-component signal whose energy is concentrated around the beat frequency that corresponds to the distance between the antenna and the probed reflecting layer. As the fluctuation level increases, the interference signal suffers phase and amplitude modulations that scatter its energy over a wider frequency range, not necessarily centered in the main beat frequency component that would correspond to the underlying non-perturbed profile. In this case the signal becomes clearly multi-component and the concept of instantaneous frequency loses its meaning. Two simple approaches to extract the beat frequency from the spectrogram have been investigated. The first and most straightforward method consists in detecting the highest valued peak of the spectrogram, for each time slice:

$$f_b(t) = \arg\max_f SPEC_h(t, f) \tag{20}$$

In the second method, the beat frequency is obtained by calculating the spectrogram's first moment:

$$f_b(t) = \frac{\int f\, SPEC_h(t, f) df}{\int SPEC_h(t, f) df} \tag{21}$$

Both approaches are efficiently implementable and do not require any special parameter adjustment. They are, therefore, ideal for an unsupervised application. However, in the presence of multi-component signals resulting from strong plasma perturbations, the first method might produce high valued

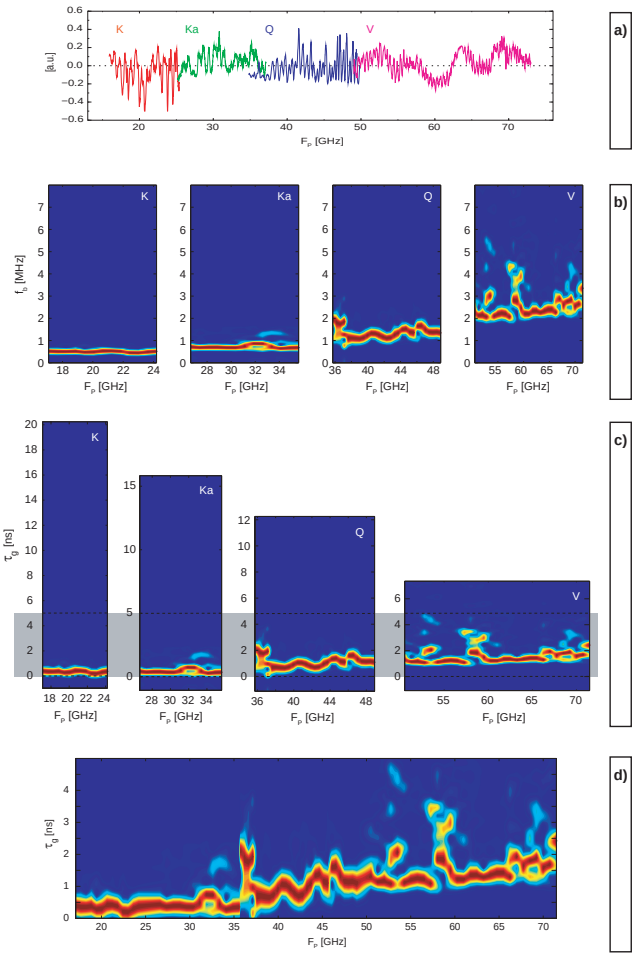

Fig. 5. Building a broadband spectrogram representation: a) raw data from 4 bands; b) individual spectrograms; c) converting the f_b axis to τ_g; d) merging, cropping and resampling the 4 spectrograms.

spurious peaks whilst the second might integrate components of non neglectable energy content into the beat frequency calculation. In the latter case, a severe bias in the estimation of f_b might occur in the more perturbed probing ranges. When calculating the density profile such spikes or long lasting biases of f_b can, in turn, result in a biased density profile reconstruction. To overcome such limitations, a shortest-path algorithm has been used to retrieve alternative f_b evolution paths from the spectrogram, taking into account the less energetic frequency peaks in the more perturbed regions. This approach was implemented in ASDEX Upgrade, for the off-line reflectometry data processing, using a Floyd-Warshall algorithm [23]. The technique allows the elimination of most of the spurious peaks of the f_b curve but is very time and resource consuming, and in general requires the supervision of an operator to adapt the algorithm parameters to the plasma regime.

The results obtained with all of these techniques can be improved by averaging the spectrograms of bursts of closely taken measurements. This procedure enhances the spectral peaks that correspond to the underlying mean density profile.

If in the time window under consideration the plasma profile is such that the consecutive measurements exhibit a high correlation level, the background noise as well as the localized measurements' phase modulations can be to some extent canceled or mitigated. The improvements obtained over single sweep group delay averaging, as well as the gained robustness to high turbulence levels, were verified using 2D FDTD full wave codes [24]. This procedure proved to be particularly effective when coupled to the simple maximum peak detection algorithm. It considerably reduces the amount of spurious f_b peaks therefore increasing the reliability of the corresponding inverted density profiles.

Density profile calculation

In O-mode propagation the lowest density layers corresponding to the frequency range $[0, \sim 17]$ GHz can not be probed. In this frequency range the wavelength of the probing waves becomes larger than the local density gradient scale length (the length of the reflecting density layer). In order to calculate the Abel inversion required to reconstruct the density profile, eq. (6), the group delay evolution that corresponds to this unprobed frequency range has to be guessed within rather loose boundaries. Bad extrapolations for these unmeasured values can easily produce large errors in the density profile reconstruction.

The inversion integral of eq. (6) can thus be decomposed in two sub-integrals:

$$x_{co}(f_{co}) = \frac{c}{\pi}\int_0^{F_{P0}} \frac{\tau_{g\_ini}(f)}{\sqrt{f_{co}^2 - f^2}} df + \\ + \frac{c}{\pi}\int_{F_{P0}}^{f_{co}} \frac{\tau_g(f)}{\sqrt{f_{co}^2 - f^2}} df \qquad (22)$$

where F_{PO} is the first probing frequency. The first term accounts for the contribution of the guessed group delay, $\tau_{g\_ini}(f)$, for $f < F_{P0}$. The second term accounts for the contribution of the measured group delay, obtained by probing the plasma with frequencies above $F_{P0} \approx 17$ GHz. The off-line profile calculation process often requires human intervention to introduce adjustments in the guessed $\tau_{g\_ini}(f)$ initialization and fine tune the filtering applied to the measured $\tau_g(f)$. Furthermore, the Abel inversion requires an highly detailed $\tau_g(f)$ input so that any spurious perturbations do not translate into severe accumulated radial reconstruction errors.

Because this higher detail is directly proportional to the amount of required time-frequency calculations, to maintain the overall number of computations at a level compatible with the control cycle, a novel approach based on the application of *machine learning* techniques was developed [25], [26]. By using a *feedforward multilayer neural network*[10] to solve, in a single step, the $\tau_{g\_ini}(f)$ initialization and the profile inversion, it was possible to use a reduced number of input group delay values, even in the presence of relatively high plasma perturbations, and still achieve the accuracy required for profile reconstruction. This particular type of *neural networks* (NN) proved to be capable of calculating the non-linear regression that corresponds to the Abel inversion, in spite of the lack of the unprobed $\tau_{g\_ini}(f)$ data. Because the NNs were trained to produce a smoothed mean profile, they inherently compensate the influence of measurement perturbations that would bias the traditional profile reconstruction procedure.

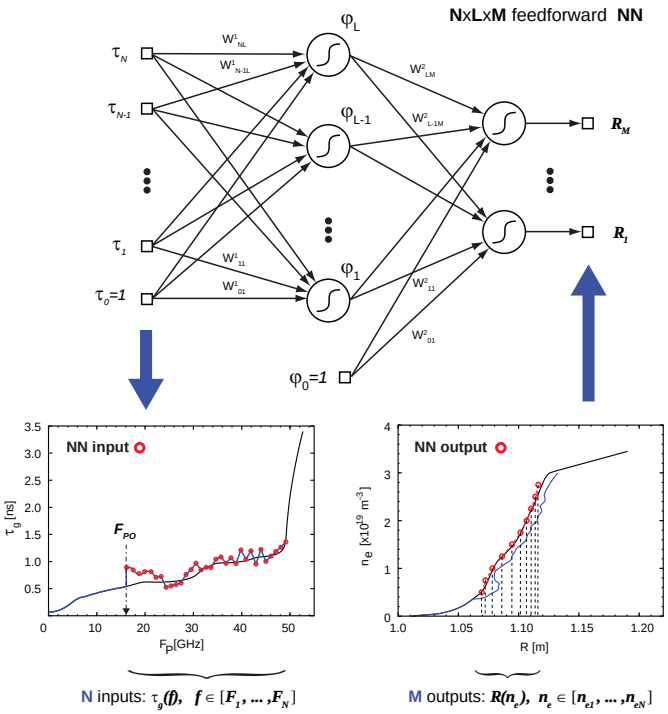

Fig. 6. Used NN topology (top). Example of the NN group delay input (red dots - left bottom plot) and resulting radial position output (red dots - right bottom plot). The wiggling profile was obtained by inverting the same noisy $\tau_g(f)$ data using the Abel inversion (blue curves).

The adopted neural network topology uses one layer of hidden units and sigmoidal activation functions. Its input is a discrete set of measured group delay values extracted from the joint multi-band TFD (Fig. 5). The NN produces the output smooth profile in the form of a set of discrete radial positions that correspond to a fixed predefined set of densities.

Fig. 6 shows the adopted NN topology and an example of a profile reconstruction based on a simulated case. The red dots, on the lower plots, represent the NN input group delay data (left) and output profile (right). In blue, the simulated perturbed group delay measurement (from which the NN input vector was sampled), and the corresponding profile when inverted using the Abel integral. The black solid lines represent the simulated mean underlying profile (and corresponding group delay) that we wish to reproduce using the neural approach. As can be seen, in this example, inverting the detailed perturbed group delay measurement, using the Abel

[10]The *universal approximation theorem for neural networks* [27] states that every continuous function that maps intervals of real numbers to some output interval of real numbers can be approximated arbitrarily closely by a single hidden layer NN, provided that a large enough number of units exist in the hidden layer. This result, however, holds only for restricted classes of activation functions such as the sigmoidal squashing functions.

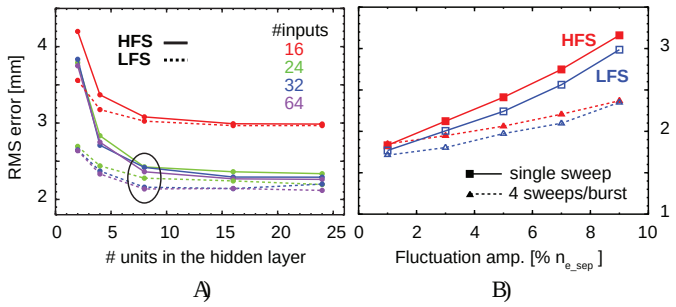

Fig. 7. a) RMS reconstruction errors obtained by changing the NN topology; b) NN performance when reconstructing test datasets affected by different levels of density fluctuations.

integration, results in an undulating profile that exhibits a radial shift in relation to the original undisturbed profile. This shift would have been greater if the $\tau_{g\_ini}(f)$ used to invert the profile was actually guessed and not the exact $\tau_g(f)$ values of the original simulated unperturbed curve. The NN, in this case, was able to produce a smoother profile that closely matches the underlying mean profile. This coarser profile representation, although not suited for detailed physics studies, is quite adequate for the plasma position control application.

The NNs learning phase, in which the popular *backpropagation algorithm* [28] was used, required an extensive dataset of perturbed group delay measurements and their respective target smooth density profiles. This database was built using profiles collected experimentally in relevant plasma discharges. For each of the original 12066 smoothed experimental profiles were created 4 perturbed versions by adding density fluctuations generated with a physically motivated model. Five different datasets were created for five density perturbation amplitudes, ranging from 1% to 9% of the density found at the magnetic separatrix position (n_{e_SEP}). Realistic reflectometry raw data, corresponding to these perturbed profiles, was then generated using a 1D finite-difference time-domain (FDTD) Full-wave code [29]. The spectrogram and maximum peak detection algorithms were applied to the simulated reflectometry raw data to produce single and burst (groups of 4 correlated measurements) group delay measurements. The resulting database of simulated perturbed group delay data and corresponding target (original) smooth profiles was used not only to train (50% of the entries) and test (the remaining 50%) the neural networks but also to assess the comparative performance between this technique and the standard inversion procedure. The complete database includes 12066 smooth profiles, 241320 perturbed profiles, 241320 single sweep and 60330 burst group delay measurements, equally divided between the HFS and LFS.

The NN topology that produced the best results was found by scanning the number of used inputs (level of discretization of the input group delay measurement) and units in the hidden layer (Fig. 7.a). The chosen NN topology was then used to train NNs with the various perturbed datasets. Fig. 7.b shows the overall RMS errors obtained when reconstructing the entire

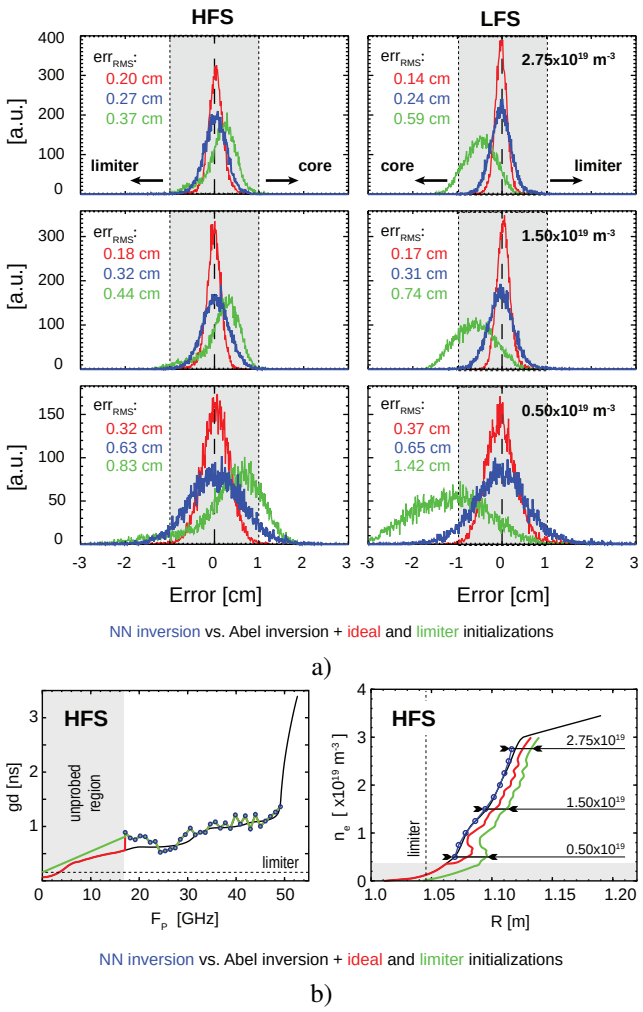

Fig. 8. a) Position error histograms of the reconstruction of a test dataset perturbed by 9% of n_{e_sep} fluctuation amplitude with a NN and the Abel inversion with the ideal and practical (limiter) initializations. b) Example of a perturbed group delay measurement and ideal and limiter initialization (left) and the corresponding inverted profiles (right).

perturbed test datasets using a NN with 24 inputs and 8 hidden units to produce a 10 point output profile, covering a $n_e = [0.5 - 2.75] \times 10^{19}\,\mathrm{m}^{-3}$ density range.

Fig. 8 shows an example of the the position error histograms, at three density layers (0.5, 1.5 and $2.75 \times 10^{19}\,\mathrm{m}^{-3}$), obtained by reconstructing the most perturbed test dataset (density fluctuations with an amplitude of 9% of n_{e_SEP}). As can be seen, the neural approach performance (blue histogram) compares well with the ideal situation where the profile is inverted using the exact $\tau_{g\_ini}(f)$ that is not measured experimentally (red histogram). The standard off-line initialization procedure consists in approximating $\tau_{g\_ini}(f)$ by a linear extrapolation between the $\tau_g(f)$ value equivalent to the position of the plasma limiting wall (also called limiter) and the first measured $\tau_g(f)$ value. This static initialization procedure produces highly biased error histograms (in green) and higher overall RMS errors.

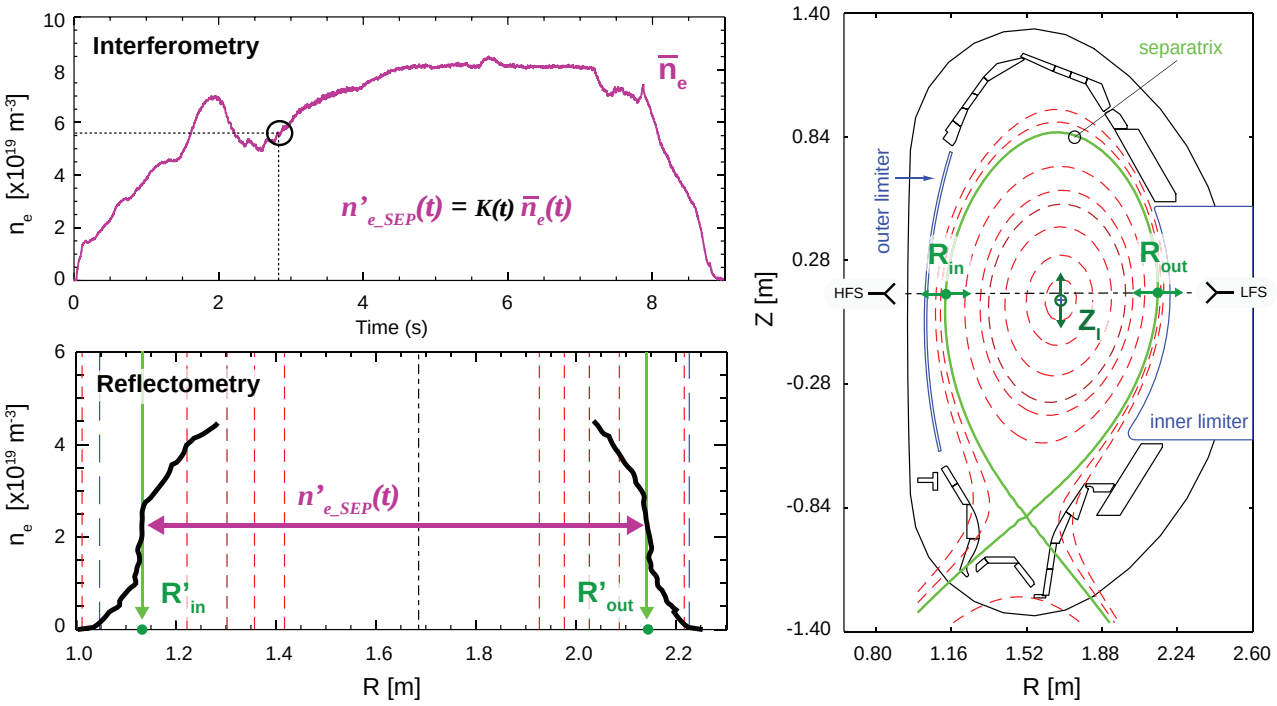

Fig. 9. Simplified view of the procedure used to obtain an estimation of the position of the magnetic separatrix (at the reflectometers' lines of sight) from the HFS and LFS density profiles. $K(t)$, on the top plot, is the regime dependent scaling used to estimate the density at separatrix.

III. Controlling the plasma position

The position control of the plasma column is made by monitoring the location of a few control points of the last closed flux surface, also known as the magnetic separatrix (green line on the right plot of Fig. 9). Based on the feedback of their locations, the position controller changes the configuration of the magnetic fields that trap the plasma inside the tokamak vessel. To be able to replace the magnetic diagnostic, reflectometry must accurately (within a 1 cm error bar) provide the controller with the same input information. However, because the separatrix results exclusively from the reconstruction of the magnetic flux distribution, no direct relation with the plasma electron density exists. Thus, a good estimation for the density just inside this flux surface is needed in order to track its approximate location from a reflectometry density profile. Fortunately, for any given tokamak and plasma regime there is an empirical scaling that relates the plasma line average density , $\bar{n}_e$, and the density at the separatrix, n_{e_sep}. In practice, the on-line estimation of the density at the separatrix is accomplished using a set of a priori known regime characteristic scaling factors and the core line integrated density[11] measurement produced by the RT interferometry system, equally non-dependent on the magnetic measurements one intends to replace. The described estimation procedure is schematically depicted in Fig. 9.

In ASDEX Upgrade, plasma position is controlled by a fast feedback loop operating in a ≈ 1 ms control cycle [30], [31]. In this fast time scale, the position controller continuously monitors the radial, R_{out}, and vertical, Z_I, coordinates of the plasma column (see poloidal cut view on Fig. 9) to calculate the required corrective feedback actuation in the control coils. In order to accomplish a full feedback control demonstration, the reflectometry outer separatrix estimations, R'_{out}, obtained using the LFS RT density profiles, must satisfy the required accuracy, i.e. 1 cm, and be produced in 1 ms, a time scale 10x faster than the one required for the future ITER PPR.

[11]In the regimes of interest and under controlled conditions this measurement can be used as a replacement for the line averaged density.

Improving the reliability of the position estimate

The target plasma scenario (ITER reference scenario), in which this redundant control system should operate flawlessly, is a high plasma confinement regime known as the ELMy H-mode. This regime is characterized by the occurrence of cyclic outbursts of particles and energy called Edge Localized Modes (ELMs). During the short transient phase (ELM collapse) in which the density profile crashes, reflectometry measurements become useless (Fig. 10). Furthermore, during the recovery phase of the ELM, the scaling factor used to estimate the density at the separatrix loses its physical validity.

For these reasons it is important to have a high profile measurement rate (when compared to the ELM frequency) and a robust mechanism to automatically discard, from the position estimation procedure, density profiles measured during these phases. As on AUG no RT ELM event signaling is available, a new automatic measurement rejection mechanism had to be developed [32]. Based on Kalman filtering, the rejection method essentially implements a predictor-corrector type of estimator which is used to remove the affected measurements

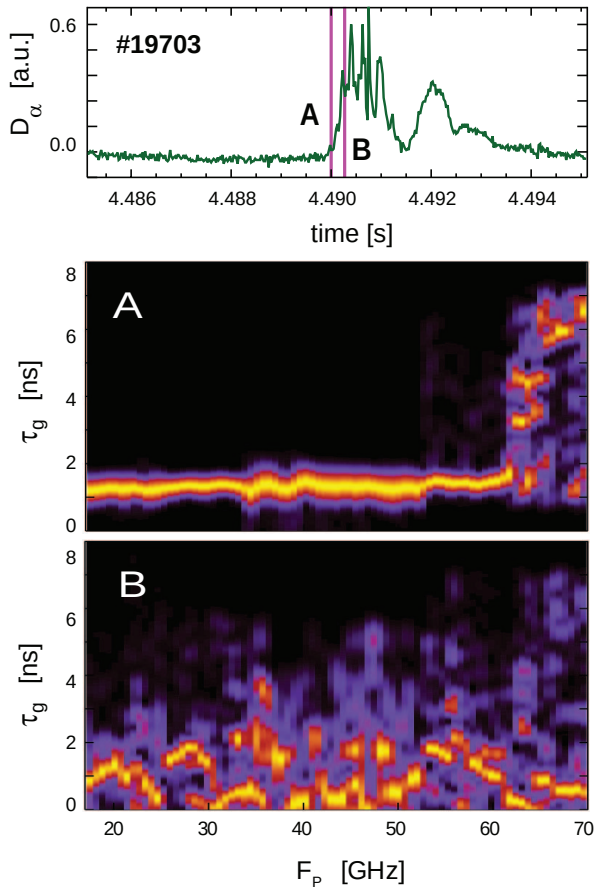

Fig. 10. α particle radiation, reaching the tokamak divertor plates, during an ELM event (top plot). Multi-band spectrograms (τ_g space) of the reflectometry signals: A - immediately before the ELM onset; B - during the ELM collapse phase.

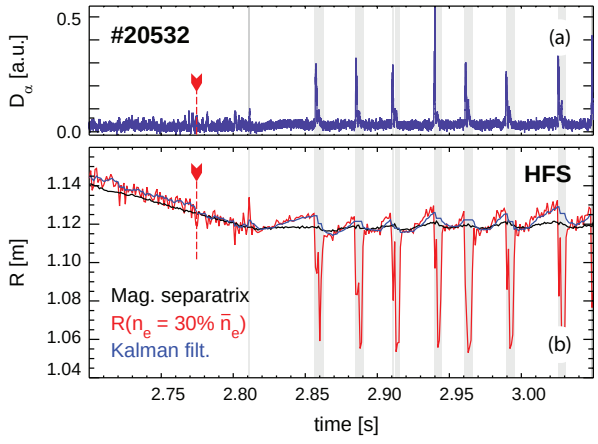

Fig. 11. Kalman based rejection/filtering algorithm used to eliminate position estimates performed during strong ELM activity (larger spikes on the red curve, bottom plot) from the actual position signal fed to the plasma position controller (blue curve, bottom plot), from [32].

from the filtered stream of estimated positions, R'_{out} (Fig. 11). The method's implementation also automatically generates confidence values associated with the position estimates fed to the position feedback controller.

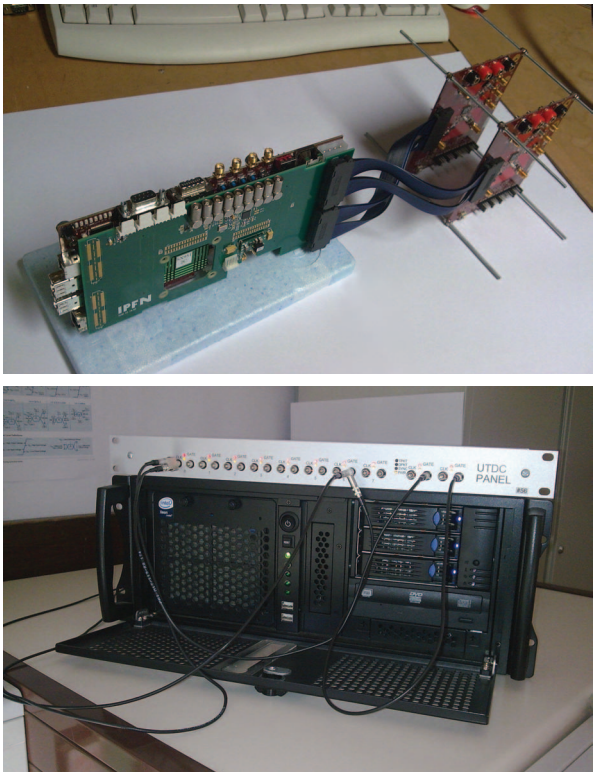

Fig. 12. Custom built 8 channel high-throughput PCIe (x8 lane bus) acquisition system (top), and hosting RT data processing diagnostic server and timing system connection bar (bottom).

Diagnostic hardware upgrades

To cope with the controller's tight timing requirements, the existing AUG reflectometry diagnostic was upgraded with a custom built high-performance data acquisition and processing system (12 and Fig. 13). A dual quad-core (Xeon E5450@3 GHz) rack-mounted server was used to host both the data acquisition system and the experiment's timing and synchronization device[12] (uTDC). This compact system is sufficiently powerful to compute in real-time (RT) the density profiles and position estimates, whilst simultaneously performing all the data communication tasks with the AUG discharge control system (DCS). The system is connected to the DCS via a dedicated Gigabit Ethernet (UDP protocol), used only by the RT diagnostics involved in the control of the machine.

The more critical element in the diagnostic upgrade, however, was the data acquisition system (DAS), which must be capable of delivering the acquired data to the data-processing resources with very low latencies and in the shortest possible time. For this purpose, a custom PCIe 1.1 (x8) DAS was designed [34] to remove all possible hardware-related latencies from the RT measurement cycle. The 8-channel (12-b/105 MSPS) DAS uses a Xilinx Virtex-5 SX series FPGA capable

[12]This in-house (IPP) designed timing device guarantees the synchronization between the discharge control system and all the RT diagnostic nodes [33].

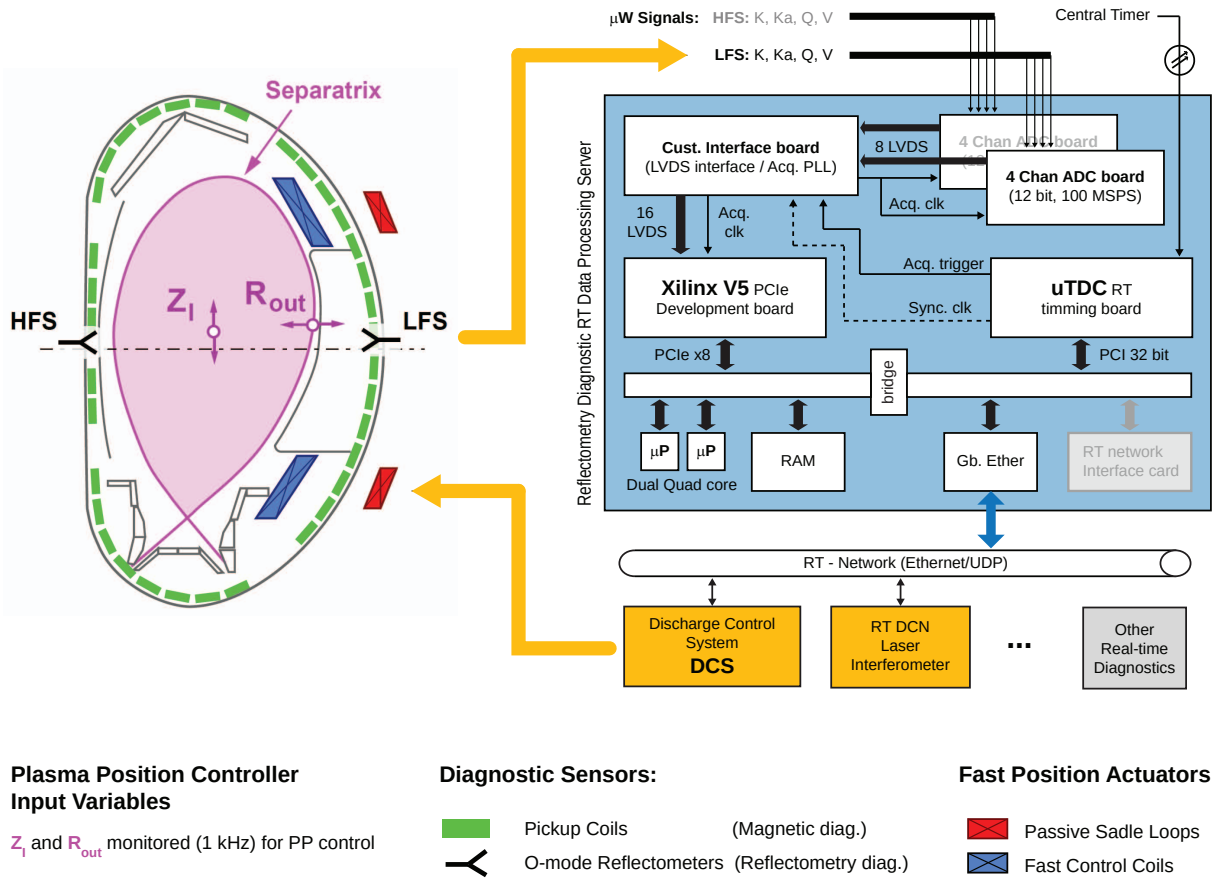

Fig. 13. Schematic diagram of the RT reflectometry diagnostic and plasma position control flow.

of sustaining DMA data burst transfers, between the local data acquisition buffering FIFO and the data processing server's RAM, with a measured effective bandwidth of 1.272 GB/s. During the system's benchmarking phase, this value only dropped below this mark on 0.2% of the cases (staying always above 908 MB/s) when one CPU (all 4 cores) was fully loaded running a system stress benchmark tool[13]: the "Calibrator v0.9e" [35], [36] (Fig. 14.a). The DMA core in the FPGA was programmed so that the DMA transfer to the host's RAM is started before the bursts of acquired data are completely available in the FPGA local FIFO buffer. In this way, in 99.8% of the times (loaded system), the transfer is completed just 1 μs after the last sample of a burst is acquired.

As the complete control cycle (1 ms) is relatively slow for modern RT systems, the operating system (OS) chosen to be installed in the server was a standard openSuse 11.2 (x86_64) distribution with a RT enabled 2.6.31.12-rt21 kernel (standard kernel with RT_PREEMPT patches applied). The choice of a RT enabled standard OS over a hard-RT commercial OS allowed for an easier integration on the existing AUG RT software infrastructure and for an higher development flexibility. The deterministic response of the system was, nevertheless, very satisfactory as the data in Fig. 14.b shows. In a loaded system, the user-space RT data processing (DP) task, running on segregated cores, could start calculating the density profiles, in 99.99% of the cases, $< 40\,\mu$s after the end of the DMA transfer, when an IRQ based mechanism was used. By polling the device driver shared DMA data buffer, this delay dropped to $< 10\,\mu$s ($< 5\,\mu$s on an idle system). No latencies higher than 70 μs were ever registered, regardless of the DP task wake up mechanism employed. Adding these latencies to the time taken to acquire each burst of reflectometry data and transfer it (DMA) into RAM never surpassed the 210 μs bar, leaving ample time for the profile based separatrix position estimation and its delivery to the DCS ($\approx 790\,\mu$s).

The high performance of the multi-core multiprocessor host directly contributed to limit the complexity programmed into the DAS embedded FPGA. All the data processing algorithms running in a RT task in user-space were implemented using optimized digital signal processing libraries and OpenMP parallel/multithreaded programming[14]. Measured computation times of $< 400\,\mu$s were obtained for the calculation of HFS and LFS RT profiles when using 4 segregated cores on the same CPU. Fig. 14.c shows how the multi-thread code performance scaled with the used number of cores (with hyper-threading disabled). The acquisition and data processing

[13]This tool constantly provokes cache misses, saturating the access to the memory bus.

[14]Using Intel C and C++ compilers and Intel IPP libraries.

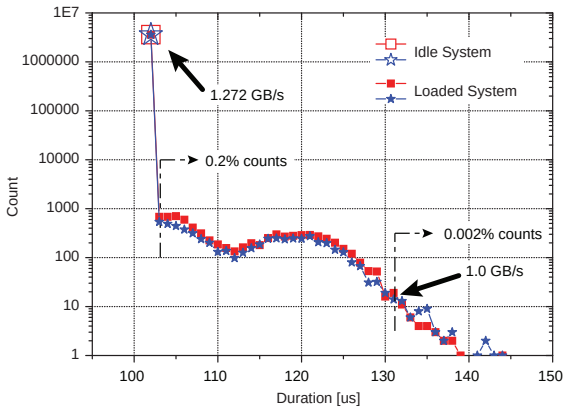

a)

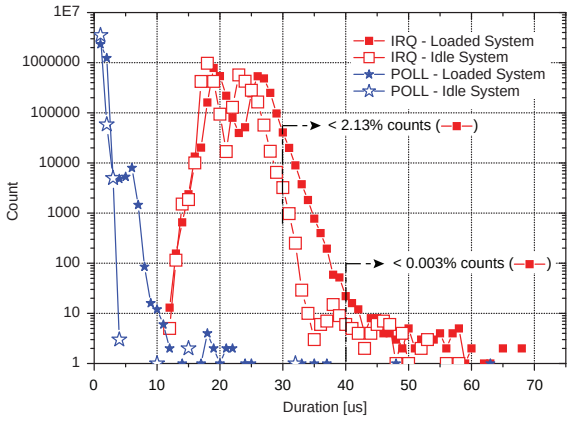

b)

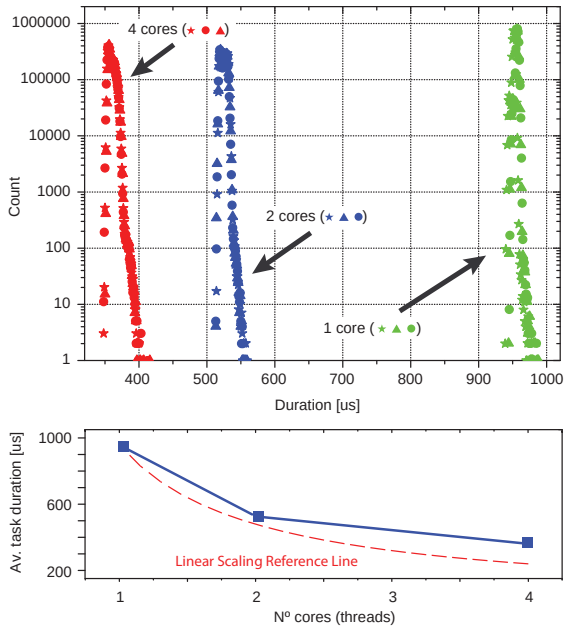

c)

Fig. 14. a) Histograms (4) of the measured DMA transfer duration (128 KiB block); b) histograms (4) of the measured user space task activation delay; c) histograms (9) of the RT data-processing task duration using 1, 2, and 4 cores and duration scaling curve with number of cores.(From [34])

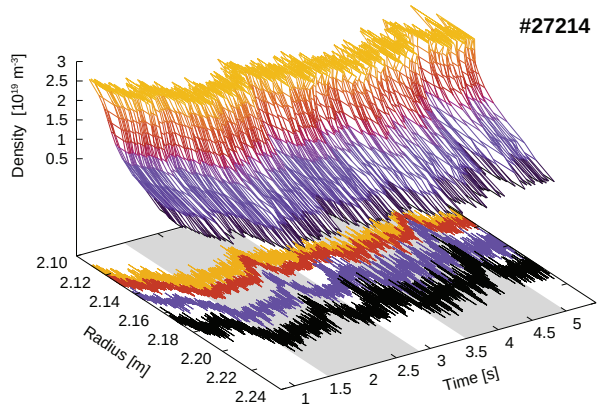

RT Profile rate: 1 ms

Each profile contains:
Data from 3 reflect. bands
Burst of four 25 µs sweeps

Total input data / profile:
12x1KB sample raw signals

Fourier analysis / profile:
24x4=96 1KB FP FFTs

Inversion NN topology:
24x8x10
(output density range 0.5-3x10^{19} m^{-3})

Fig. 15. Automatically validated LFS RT reflectometry profiles, produced during the #27214 demonstration discharge.

threads were integrated in the standard AUG RT diagnostic software framework [37] that handles all the synchronization and RT communication with the DCS. In Fig. 15 are shown the LFS RT profiles produced in one of the demonstration discharges and information (box) corresponding to the amount of data and floating point operations involved in their calculation.

IV. The Feedback Control Demonstration

At the end of AUG's 2011 experimental campaign, the integration of the upgraded diagnostic in the AUG's RT diagnostic network was completed and the connection to the DCS tested. On the discharges dedicated to the plasma position feedback control demonstration, the performance of the developed systems and RT algorithms was tested in both L[15] and ELMy Hmode regimes [38]. The switch between magnetic and reflectometry based controllers was tested in discharges #27213 and #27214. The top left plot of Fig. 16 shows the time traces of the position controller target trajectory (black curve) and of the magnetic (green) and reflectometric (red) separatrix positions of discharge #27214. During this discharge, the radial position control was switched from magnetic to reflectometry input measurements during two separate time intervals: 1.5-2.8s and 3.5-5s (shaded periods). These intervals correspond to L-mode and ELMy H-mode phases, respectively. The controller, whose settings were still adjusted for the standard magnetic control, was able to actuate the coils so that the outer plasma radial position closely followed the control reference trajectory during the two different plasma regimes. In the second demonstration discharge, #27372 (right plots of Fig. 16), performed using the reflectometry based controller throughout L and Hmode

[15]The L-Mode is a lower confinement, ELM free, plasma regime.

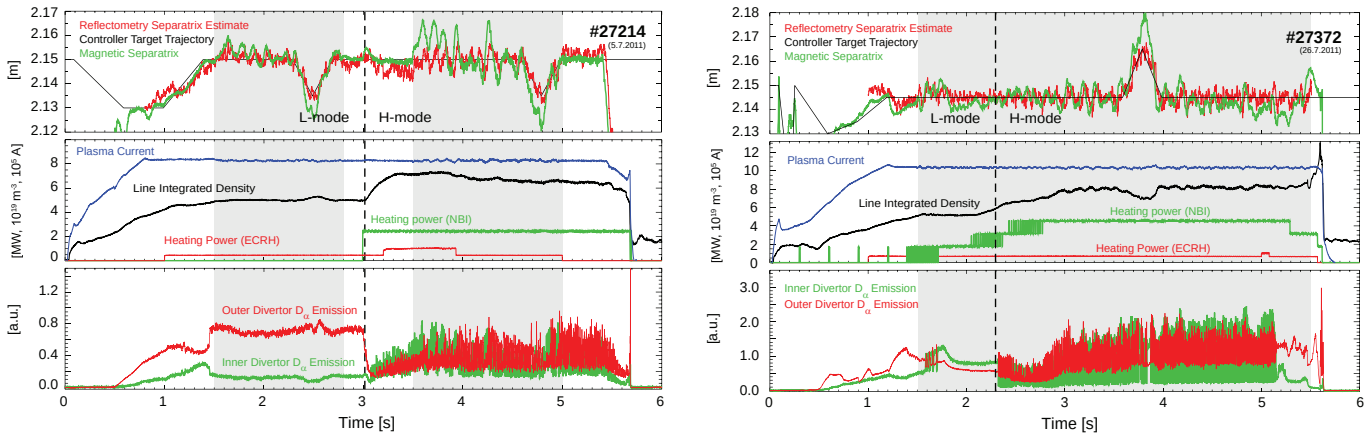

Fig. 16. Time traces of the position controller target trajectory and of the magnetic and reflectometric separatrix positions (reflectometry based control was performed during the shaded periods) in demonstration discharges #27214 and #27372.(From [38])

phases (between t = 1.5 s and t = 5.5 s) without interruptions, the scaling used to infer the separatrix position was changed online at a pre-programmed time. As there are no reliable RT regime identification signals that could be used online, this instant was chosen to roughly coincide with the expected L-H transition. The controller coped with all the transitions between the two input sources, magnetic and reflectometric, always maintaining the controlled position close to the programmed trajectories. Taking into account that, in these first feedback control experiments, the controller settings were still adjusted for the standard magnetic control, the obtained results are a clear evidence of the reflectometry based approach robustness.

Presently, work is underway to improve the performance of this control approach. The dynamics of the density based position estimates and of the indirect physical interaction between the controllable confining magnetic field and the observable density evolution are being incorporated into the controller's transfer function. The HFS density profile measurements and separatrix position estimates, not used in this demonstration, will be used in the near future either in a more sophisticated position control scheme or for shape[16] control (AUG shape controller uses both Rin and Rout separatrix position input signals - see Fig. 9).

V. Conclusion

With the demonstration of this novel control method, we proved, for the first time, that microwave radar diagnostic techniques can be used as an alternative to standard magnetic measurements for plasma position control. With this new method, we are actively contributing to the increase of the high availability and reliability levels required for the operation of ITER, helping to pave the way towards the realization of future fusion power plants.

The relevance of this demonstration to the international efforts to built ITER is evidenced by the priority support granted to the project by the European Fusion Development Agreement (EFDA)[17] and by the award of the contract[18] for the design of the ITER Plasma Position Reflectometer to a consortium led by the Portuguese IPFN/IST team, in the frame of an international call launched by Fusion for Energy (F4E).

[16]The geometric configuration of the separatrix.

Acknowledgment

This work, supported by the European Communities and the Instituto Superior Técnico, has been carried out within the Contract of Association between EURATOM and IST. Financial support was also received from the Fundação para a Ciência e Tecnologia in the frame of the Contract of Associated Laboratory. The views and opinions expressed herein do not necessarily reflect those of the European Commission, IST and FCT.

References

[1] A. Silva, L. Cupido, M. Manso, F. Serra, I. Nunes, J. Santos, P. Varela, S. Vergamota, L. Meneses, V. Grossman, F. Silva, C. Loureiro, F. Nunes, B. Kurzan, and W. Suttrop, "Microwave reflectometry diagnostic for density profile and fluctuation measurements on ASDEX Upgrade," *Review of Scientific Instruments*, vol. 70, no. 1, pp. 1072–1075, 1999. [Online]. Available: http://dx.doi.org/doi/10.1063/1.1149439

[2] J. Santos, "Reflectometry measurements for plasma position control purposes," Ph.D. dissertation, Dep. Electrical Engineering - Instituto Superior Técnico, Av. Rovisco Pais, 1049-001 Lisboa, Portugal, May 2008.

[3] K. C. Yeh and C. H. Liu, *Theory of Ionosferic Waves*. Academic Press, 1972.

[4] V. L. Ginzburg, *The Propagation of Electromagnetic Waves in Plasmas*, 2nd ed. Pergamon Press, 1970.

[5] I. H. Hutchinson, *Principles of Plasma Diagnostics*. Cambridge University Press, 1987.

[6] F. Simonet, "Measurement of electron density profile by microwave reflectometry on tokamaks," *Review of Scientific Instruments*, vol. 56, no. 5, pp. 664–669, 1985.

[7] S. W. Smith, *The Scientist and Engineer's Guide to Digital Signal Processing*, 2nd ed. California technical Publishing, 1999.

[8] A. Silva, "The ASDEX Upgrade broadband microwave reflectometry system," Ph.D. dissertation, Instituto Superior Técnico, 2006.

[9] J. Doane, E. Mazzucato, and G. Schmidt, "Plasma density measurements using FM-CW milimeter wave radar techniques," *Review of Scientific Instruments*, vol. 52, no. 1, pp. 12–15, January 1981.

[17]EFDA Tasks WP08/09-DIA-01-01 and WP10-DIA-03-01.

[18]Framework Partnership Agreement contract F4E-FPA-375 (DG).

[10] A. Silva, P. Varela, L. Cupido, M. Manso, L. Meneses, L. Guimarais, G. Conway, F. Serra, and T. ASDEX Upgrade Team, "Automatic electron density measurements with microwave reflectometry during highdensity H-mode discharges on asdex upgrade," in *Proceedings of the* 7^{th} *International Reflectometry Workshop*, Garching, May 2005.

[11] B. Boashash, "Estimating and interpreting the instantaneous frequency of a signal-Part 1: Fundamentals," *Proceedings of the IEEE*, vol. 80, no. 4, pp. 520–538, April 1992.

[12] E. J. Doyle, T. Lehecka, N. Luhmann Jr., , and W. Peebles, "X-mode broadband reflectometric density profile measurements on diii-d," *Review of Scientific Instruments*, vol. 61, no. 10, pp. 2896–2898, October 199.

[13] M. Manso, A. Silva, F. Serra, J. Matias, F. Soldner, L. Cupido, J. Pereira, J. Neves, F. Nunes, L. Leitao, P. Varela, A. Moreira, C. Fernandes, C. Correia, C. Loureiro, and J. Santos, "Fast sweep multiple broadband reflectometers on asdex and asdex-upgrade," in *Proceedings of the IAEA Technical Committe Meeting: Microwave Reflectometry for Fusion Plasma Diagnostics*, IAEA, Ed. JET, 1992, pp. 1–10.

[14] A. Silva, L. Cupido, M. Manso, P. Varela, F. Serra, and A. U. Team, "Continuous phase derivative evaluation for density profile measurements from FM broadband reflectometry," in *Proceedings of the* 22^{nd} *EPS Conference on Controlled Fusion and Plasma Physics*, B. Keen, P. Stott, and J. Winter, Eds., vol. 19C. Bournemouth: European Physical Society, 1995, pp. 413–416.

[15] E. Kim, K.W. Doyle, W. Peebles, A. Ejiri, N. Luhmann Jr., and C. Rettig, "Advances in reflectometric density profile measurements on the DIII-D tokamak," *Review of Scientific Instruments*, vol. 66, no. 2, pp. 1229–1232, February 1995.

[16] J. Bizarro and A. Figueiredo, "On complex demodulation and time-frequency distributions for broadband reflectometry signals," *Review of Scientific Instruments*, vol. 70, no. 1, pp. 1030–1033, January 1999.

[17] J. Santos, M. Manso, F. Nunes, I. Nunes, A. Silva, and P. Varela, "New data processing techniques for profile evaluation from broadband FM reflectometry," in *Proceedings of the* 3^{rd} *Workshop on Microwave Reflectometry for Fusion Plasma Diagnostics*, J. Sanchez and E. d. l. Luna, Eds. Madrid: CIEMAT, November 1997, pp. 55–64.

[18] C. Laviron, P. Moreau, F. Clairet, J. Chareau, and M. Paume, "Reflectometry measurements on the Tore Supra tokamak," in *Proceedings of the 3rd Workshop on Microwave Reflectometry for Fusion Plasma Diagnostics*, Madrid, 1997, p. 119.

[19] M. Nagatsu, A. Fuse, and A. Mase, "Application of maximum entropy method to density profile measurement via microwave reflectometry on GAMMA 10," *Plasma Phys. Control. Fusion*, vol. 38, pp. 1033–1042, 1996.

[20] L. Bruskin, A. Mase, T. Tokuzawa, N. Oyama, A. Itakura, and T. Tamano, "Measurement of plasma density using wavelet analysis of microwave reflectometer signal," *Review of Scientific Instruments*, vol. 69, no. 2, pp. 425–430, 1998.

[21] F. Nunes, M. Manso, I. Nunes, J. Santos, A. Silva, and P. Varela, "On the application of the Wigner-Ville distribution to broadband reflectometry," *Fusion Engineering and Design*, vol. 43, pp. 441–449, January 1999.

[22] J. Bizarro and A. Figueiredo, "The Wigner distribution as a tool for time-frequency analysis of fusion plasma signals: application to broadband reflectometry signals," *Nuclear Fusion*, vol. 39, no. 1, pp. 61–82, January 1999.

[23] P. Varela, M. Manso, I. Nunes, J. Santos, F. Nunes, A. Silva, and F. Silva, "Automatic evaluation of plasma density profiles from microwave reflectometry on ASDEX Upgrade based on the time-frequency distribution of the reflected signals," *Review of Scientific Instruments*, vol. 70, no. 1, pp. 1060–1063, January 1999.

[24] F. Silva, S. Heuraux, P. Varela, and M. Manso, "2D reflectometry simulation as a tool for evaluating data processing capabilities," in *Proceedings of the* 6^{th} *International Reflectometry Workshop*, San Diego, May 2003.

[25] J. Santos, F. Nunes, M. Manso, and I. Nunes, "Neural network evaluation of reflectometry density profiles for control purposes," *Review of Scientific Instruments*, vol. 70, no. 1, p. 1047, 1999.

[26] J. Santos, F. Nunes, M. Manso, and P. Varela, "A neural network approach to evaluate density profiles from reflectometry in ASDEX Upgrade discharges with internal barriers," *Fusion Engineering and Design*, vol. 48, no. 18, pp. 119–126, August 2000.

[27] K. Hornik, "Multilayer feedforward neural networks are universal approximators," *Neural Networks*, vol. 2, pp. 359–366, 1989.

[28] D. E. Rumelhart, G. E. Hinton, and R. J. Williams, *Learning internal representations by error propagation*. Cambridge, MA, USA: MIT Press, 1986.

[29] S. Hacquin, F. Silva, S. Heuraux, M. Colin, G. Leclerc, M. Manso, T. Ribeiro, J. Santos, and F. Serra, "1D and 2D full-wave simulations of o-mode reflectometry experiments in the presence of non-coherent fluctuations," in *Proceedings of the* 28^{th} *European Conference on Controlled Fusion and Plasma Physics*, vol. 25B. Funchal, Madeira: European Physical Society, June 2001, pp. 1209–1212.

[30] W. Treutterer, J. Gernhardt, O. Gruber, P. McCarthy, G. Raupp, U. Seidel, and the ASDEX Upgrade Team, "Plasma shape control design in ASDEX Upgrade," in *Proceedings of the* 19^{th} *Symposium on Fusion Technology*, vol. 1, Lisbon, 1997, pp. 933–936.

[31] W. Treutterer, G. Neu, G. Raupp, D. Zasche, and T. Zehetbauer, "ASDEX Upgrade's new plasma control scheme," *Fusion Engineering and Design*, vol. 81, no. 15-17, pp. 1927–1931, 2006. [Online]. Available: http://www.sciencedirect.com/science/article/pii/S0920379606000664

[32] J. Santos, L. Guimarais, M. Manso, and the ASDEX Upgrade Team, "Real-time reflectometry measurement validation in H-mode regimes for plasma position control," *Review of Scientific Instruments*, vol. 81, no. 10, p. 10D926, 2010. [Online]. Available: http://dx.doi.org/doi/10.1063/1.3499640

[33] A. Lohs, K. Behler, K. Lüddecke, G. Raupp, and T. A. U. Team, "The ASDEX upgrade UTDC and DIO cards - a family of PCI/cPCI devices for real-time DAQ under Solaris," *Fusion Engineering and Design*, vol. 81, pp. 1859–1862, July 2006.

[34] J. Santos, M. Zilker, L. Guimarais, W. Treutterer, C. Amador, M. Manso, and the ASDEX Upgrade Team, "COTS-based high-data-throughput acquisition system for a real-time reflectometry diagnostic," *IEEE Transactions on Nuclear Science*, vol. 58, no. 4, pp. 1751–1758, August 2011. [Online]. Available: http://dx.doi.org/doi/10.1109/TNS.2011.2143428

[35] S. Manegold and P. Boncz, "Cache-memory and tlb calibration tool," Tech. Rep., 2004. [Online]. Available: http://homepages.cwi.nl/ manegold/Calibrator/doc/calibrator.pdf

[36] S. Manegold, "The calibrator (v0.9e), a cache-memory and tlb calibration tool," Tech. Rep., 2004. [Online]. Available: http://www.cwi.nl/ manegold/Calibrator/

[37] M. Reich, K. Behler, R. Drube, L. Giannone, A. Kallenbach, A. Mlynek, J. Stober, W. Treutterer, and the ASDEX Upgrade Team, "Real-time diagnostics and their applications at ASDEX upgrade," *Fusion Science and Technology*, vol. 58, no. 3, pp. 727–732, November 2010.

[38] J. Santos, L. Guimarãis, M. Zilker, W. Treutterer, M. Manso, and the ASDEX Upgrade Team, "Reflectometry-based plasma position feedback control demonstration at asdex upgrade," *Nuclear Fusion*, vol. 52, no. 3, p. 032003, March 2012. [Online]. Available: http://dx.doi.org/10.1088/0029-5515/52/3/032003